

# Potential field migration for rapid 3D imaging of entire gravity gradiometry surveys

Michael S. Zhdanov,<sup>1,2</sup> Xiaojun Liu<sup>1</sup> and Glenn Wilson<sup>2\*</sup>

## Abstract

The geological interpretation of gravity gradiometry data is challenging. With the exception of the vertical gradient, maps of the different gravity gradients are often complicated and cannot be directly correlated with geological structure. 3D inversion has been the only practical tool for the quantitative interpretation of gravity gradiometry data. However, it is a complicated and time-consuming procedure that is very dependent on the initial model and constraints used. To overcome these difficulties for the initial stages of an interpretation workflow, we introduce the concept of potential field migration and demonstrate its application for rapid 3D imaging of entire gravity gradiometry surveys. This method is based on the direct integral transformation of the observed gravity gradients into a subsurface density distribution that can be used for interpretation, or as an initial model for subsequent 3D regularized inversion. We present a case study for the interpretation of gravity gradiometry data acquired in the Nordkapp Basin. We find agreement between the results obtained from potential field migration and those obtained from 3D regularized inversion, and show that the migration results are comparable to smooth inversion. For regional-size datasets, runtimes for migration are in the order of minutes compared to hours for inversion.

## Introduction

Gravity gradiometry has come to be routinely integrated into exploration workflows, since it can provide an independent measure of the subsurface density distribution. 3D density models derived from gravity gradiometry data are used to improve velocity models used in seismic imaging of complex salt and basalt structures. The advantage of gravity gradiometry over other gravity methods is that the data are extremely sensitive to localized density contrasts within regional geological settings. High quality data can be acquired from either airborne or shipborne platforms over very large areas for relatively low cost.

A number of publications have discussed the use of 3D regularized inversion with both smooth (e.g., Li, 2001) and focusing (e.g., Zhdanov et al., 2004) stabilizers for the interpretation of gravity gradiometry data. A variety of fast imaging techniques related to Euler decomposition have also been developed. Most of these are based on the superposition of analytical responses from specific sources (e.g., Fedi, 2007). These imaging methods typically estimate the positions and some parameters of the sources based on field attenuation characteristics.

In this paper, we present a different approach to imaging based on the idea of potential field migration as originally introduced by Zhdanov (2002). The new approach provides a rapid method for direct transformation of the observed gravity gradiometry data into a 3D density distribution.

Migration can be mathematically described as the action of the adjoint operator on the observed data. This concept has been

long developed for seismic wavefields (e.g., Schneider, 1978; Berkhout, 1980; Claerbout, 1985), and was also developed for electromagnetic fields (Zhdanov, 1988, 2002, 2009), where the adjoint operators manifest themselves as the (backward) propagation of seismic or electromagnetic fields in reverse time. As applied to potential fields, such as gravity and magnetic fields, migration manifests itself as a special form of downward continuation of the potential field and/or its gradients. This downward continuation is applied to the auxiliary field obtained by moving the sources of the true observed field into the upper half-space as the mirror images of the true sources. This transformation results in extrapolation of the field downward and, contrary to conventional downward continuation, away from the mirror images of the sources. Thus migration is a stable transformation similar to conventional upward continuation. As we will demonstrate in this paper, the migration field does contain remnant information about the original source distribution, which is why it can be used for subsurface imaging.

## Potential field migration of gravity fields and their gradients

The principles of potential field migration were first described by Zhdanov (2002), where the migration was introduced as the application of the adjoint gravity operator to the complex intensity of the observed gravity field. Below, we present the formulation of 2D potential field migration for intuitive purposes, since potential field theory is far more elegant in

<sup>1</sup> The University of Utah, 1450 East, 100 South, Salt Lake City, UT 84102, USA.

<sup>2</sup> TechnoImaging, 4001 South, 700 East, Suite 500, Salt Lake City, UT 84107, USA.

\* Corresponding author, Email: glenn@technoimaging.com

2D. However, the subsequent case study will show that the method can be generalized to 3D. Though we will focus our attention on the potential field migration of gravity fields and their gradients, we note that this method can also be generalized and applied to magnetic fields and their gradients.

For a 2D gravity field represented by horizontal and vertical components  $g_x$  and  $g_z$ , respectively, we can define the complex intensity as

$$g(\zeta) = -g_x(x, z) + ig_z(x, z), \quad (1)$$

where  $\zeta = x + iz$  is a complex coordinate of the point  $(x, z)$  in the vertical plane. This satisfies the equation

$$g(\zeta') = A_g(\rho) = -2\gamma \iint_S \frac{1}{\zeta - \zeta'} \rho(\zeta) ds, \quad (2)$$

where  $\gamma$  is the universal gravitational constant,  $\rho(\zeta) = \rho(x, z)$  is a density, and  $A_g(\rho)$  denotes the forward operator for the gravity field.

We can introduce the adjoint operator of the gravity field applied to a complex function  $f(\zeta')$  as

$$A_g^*(f) = 2\gamma \int_{-\infty}^{\infty} \frac{f^*(x')}{x' - \zeta} dx'. \quad (3)$$

Similarly, for the gravity gradients represented by components  $g_{zz}$  and  $g_{zx}$  respectively, we can define the complex intensity of the gravity gradients as a complex derivative of the complex intensity of the gravity field:

$$g_T(\zeta') = \frac{\partial}{\partial \zeta} g(\zeta) = g_{zz}(x, z) + ig_{zx}(x, z), \quad (4)$$

where we have taken into account the symmetry of the gravity gradients and the fact that the gravity potential satisfies Laplace's equation. The complex intensity of the gravity gradients satisfies the equation

$$g_T(\zeta') = A_T(\rho) = -2\gamma \int_S \frac{1}{(\zeta - \zeta')^2} \rho(\zeta) ds, \quad (5)$$

where  $A_T(\rho)$  denotes the forward operator of the gravity gradients. We can introduce the adjoint operator of the gravity gradients applied to a complex function  $f(\zeta')$  as

$$A_T^*(f) = -2\gamma \int_L \frac{f^*(\zeta')}{(\zeta - \zeta')^2} d\zeta'. \quad (6)$$

The potential field migration of the gravity field is introduced as the application of the adjoint gravity operator to the complex intensity of the observed gravity field:

$$g_g^m(\zeta) = \frac{i}{4\pi\gamma} A_g^* g_g(\zeta). \quad (7)$$

If the profile of observed gravity fields coincides with the horizontal axis, then the actions of the adjoint gravity operator are equivalent to downward continuation of the complex conjugate of the observed gravity fields. Similarly, the adjoint gravity gradient operator is equivalent to the derivative of

the downward continuation of the complex conjugate of the observed gravity gradients:

$$g_T^m(\zeta) = \frac{\partial}{\partial \zeta} g_T^*(\zeta) = \frac{i}{4\pi\gamma} A_T^* g_T(\zeta). \quad (8)$$

Migration of the gravity field requires downward continuation only, whereas migration of the gravity gradients involves an additional differential operation. From a physical point of view, the migration fields are obtained by moving the sources of the observed fields above their profile as the mirror images of the true sources, because we apply the downward continuation to the complex conjugate of the observed gravity fields. The migration fields contain remnant information about the original sources of the gravity fields and their gradients, and thus can be used for subsurface imaging.

There is a significant difference between conventional downward continuation and migration of the gravity fields and their gradients. In particular, the observed gravity fields and their gradients have singular points in the lower half-space associated with their sources. Hence, downward continuation is an ill-posed and unstable transformation, as the gravity fields and their gradients can only be continued down to these singularities (e.g., Strakhov, 1970; Zhdanov, 1988). In contrast, the migration fields are analytic everywhere in the lower half-space and the migration itself is a well-posed and stable transformation.

Direct application of adjoint operators to the observed gravity fields and/or their gradients does not produce adequate imaging of the subsurface density distributions. In order to image the sources of the gravity fields and their gradients at the correct depths, an appropriate spatial weighting operator needs to be applied to the migration fields. For the gravity migration field, we can derive the gravity migration density,

$$\rho_g^m(\zeta) = -4\pi\gamma k_g w_g^{-2}(z) \text{Re} [ig_g^m(\zeta)], \quad (9)$$

which is proportional to the spatially weighted real part of the gravity migration field, where  $k_g$  is a scalar function and the weighting function  $w_g$  is proportional to the integrated sensitivity of the gravity fields (Zhdanov, 2002). Thus, the migration transformation with spatial weighting provides a stable algorithm for evaluating the gravity migration density. Likewise for the gravity gradients, we can derive the gravity gradient migration density,

$$\rho_T^m(\zeta) = -4\pi\gamma k_T w_T^{-2}(z) \text{Re} [ig_T^m(\zeta)], \quad (10)$$

which is proportional to the spatially weighted real part of the gravity gradient migration field, where  $k_T$  is a scalar function and the weighting function  $w_T$  is proportional to the integrated sensitivity of the gravity gradients (Zhdanov, 2002).

To demonstrate the effectiveness of potential field migration of noisy gravity gradiometry data, we consider profiles of  $g_{zz}$  and  $g_{zx}$  data above two infinitely long rectangular prisms with a density of 1 g cm<sup>3</sup> located 100 m below the surface (Figure 1, middle panel). With no noise added to the data, the

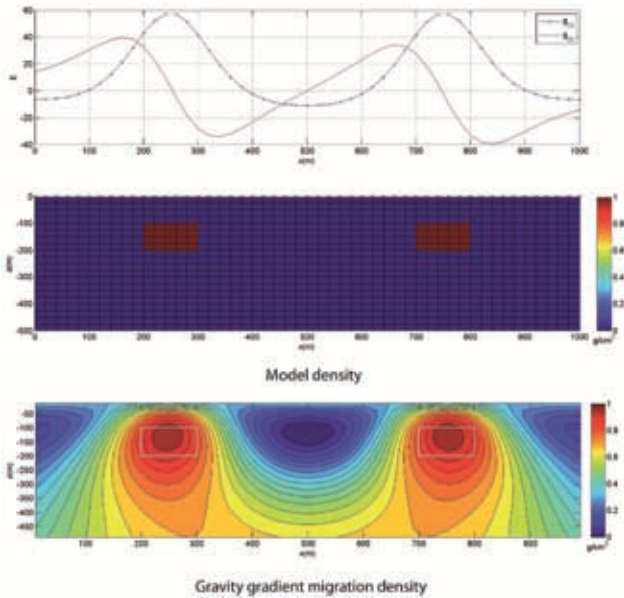


**Figure 1** Top panel: profiles of the gravity gradient components  $g_{zz}(x,0)$  and  $g_{zx}(x,0)$  along strike of two long prisms, each with a density contrast of  $1 \text{ g cm}^{-3}$ . Middle panel: vertical section of the model density distribution. Lower panel: 2D gravity gradient migration density.

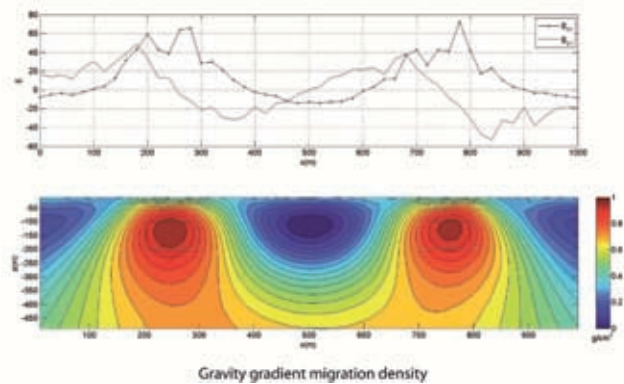


**Figure 2** Top panel: profiles of the gravity gradient components  $g_{zz}(x,0)$  and  $g_{zx}(x,0)$  with 10% random Gaussian noise added along strike of two long prisms, each with a density contrast of  $1 \text{ g cm}^{-3}$ . Lower panel: 2D gravity gradient migration density with the outlines of the two prisms.

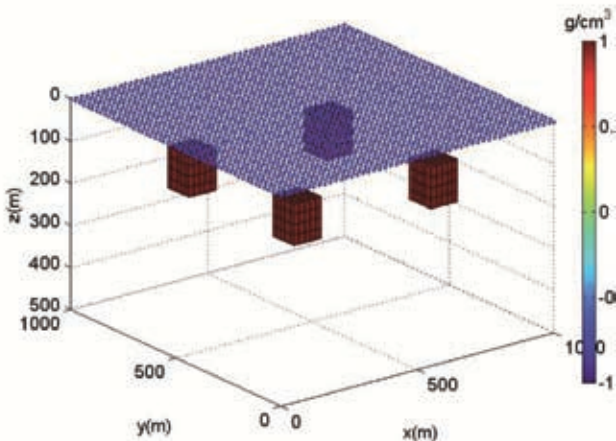


**Figure 3** 3D model of four independent bodies, each with a  $1 \text{ g cm}^{-3}$  density contrast. The observation points for  $g_{zz}(x,y,0)$  data are shown in blue.

2D gravity gradient migration density is shown in the lower panel of Figure 1, along with the outlines of the two prisms. We then added 10% random Gaussian noise to the data (Figure 2, top panel). The 2D gravity gradient migration density is shown in the lower panel of Figure 2. Clearly, the gravity gradient migration method is quite resilient, and can provide high quality images of the density distribution for noisy data.

The examples in Figures 1 and 2 have shown potential field migration in 2D. However, this method can naturally be extended to 3D. For example, we can consider the 3D potential field migration of  $g_{zz}(x,y,0)$  data as would be measured over four independent bodies of  $1 \text{ g cm}^{-3}$  density contrast (Figure 3). We have applied a joint 3D migration transformation to these data. The 3D gravity gradient migration density with a cut-off greater than  $0.8 \text{ g cm}^{-3}$  is shown in Figure 4.

### Case study – Nordkapp Basin

The Nordkapp Basin is located in the Norwegian sector of the Barents Sea (Figure 5). It is an intracontinental salt basin containing over 30 salt structures of an Early Permian age mobilized by Early Triassic sedimentation. Tertiary uplift and erosion removed nearly 1400 m of Cretaceous and younger sediments (Nilsen et al., 1995). The petroleum plays are mainly salt-related traps. Only two wells have been drilled in the basin. The Pandora well resulted in a discovery, and the Uranus well

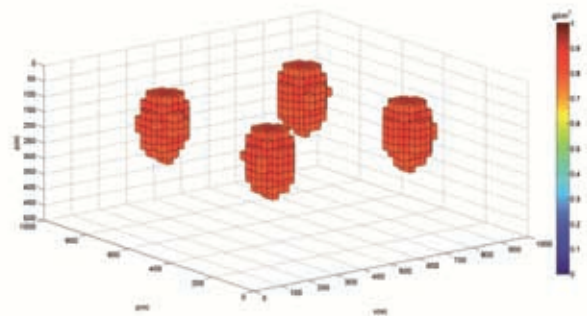


**Figure 4** 3D image of the 3D gravity gradient migration density with a cut-off greater than  $0.8 \text{ g cm}^{-3}$  density contrast.  $g_{zz}(x,y,0)$  data from the model shown in Figure 3 were migrated.

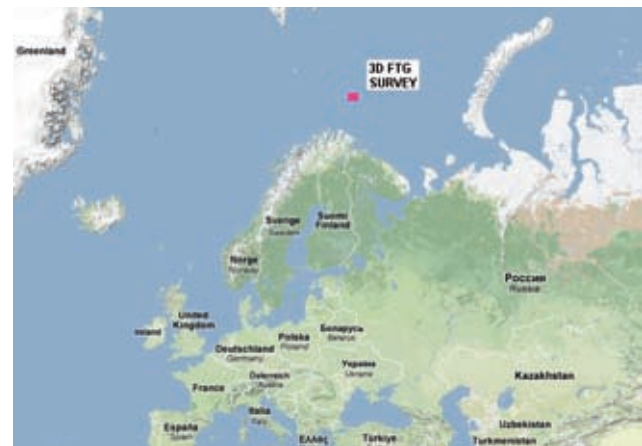


**Figure 5** Location of a full tensor gradient survey in the Nordkapp Basin in the Norwegian sector of the Barents Sea.

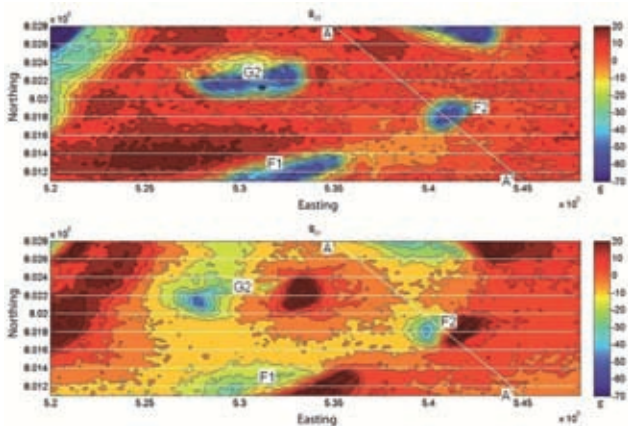


**Figure 6** Maps of  $g_{zz}$  and  $g_{zx}$  survey data for the Obelix prospect in the Nordkapp Basin. Salt diapirs G2, F1 and F2 are shown. Profile lines are also marked in white.

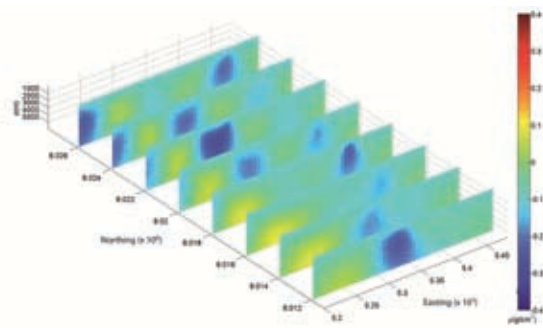


**Figure 7** 2D vertical cross-sections of density contrasts in the Nordkapp Basin obtained from 3D gravity gradiometry migration for all 48,051 stations of  $g_{zz}$ ,  $g_{yy}$  and  $g_{zx}$  data. This result was obtained in approximately 1 minute on a desktop PC running 32 bit Windows XP with a 2.4 GHz serial processor and 4 GB of RAM.

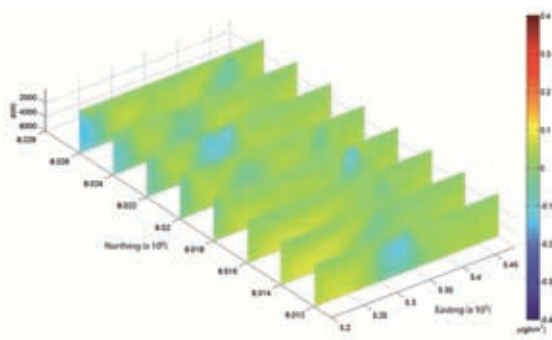


**Figure 8** 2D vertical cross-sections of density contrasts in the Nordkapp Basin obtained from 3D smooth inversion of  $g_{zz}$ ,  $g_{yy}$  and  $g_{zx}$  data. This result was obtained in 3.4 hours on a desktop PC running 32 bit Windows XP with a 2.4 GHz serial processor and 4 GB of RAM.

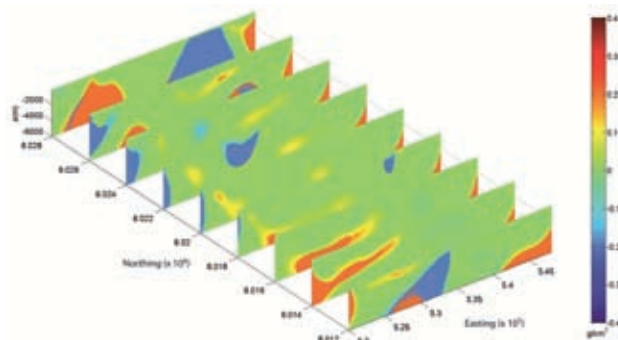


**Figure 9** 2D vertical cross-sections of density contrasts in the Nordkapp Basin obtained from 3D focusing inversion of  $g_{zz}$ ,  $g_{yy}$  and  $g_{zx}$  data. This result was obtained in 25.2 hours on a desktop PC running 32 bit Windows XP with a 2.4 GHz serial processor and 4 GB of RAM.

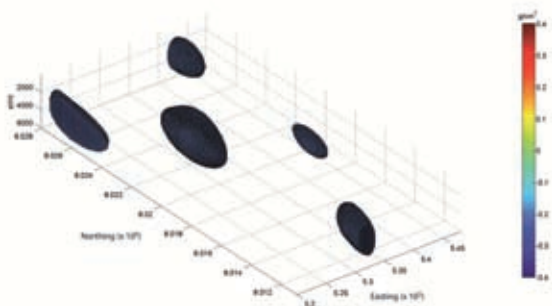


**Figure 10** Volume image of the results of 3D gravity gradiometry migration for all 48,051 stations of  $g_{zz}$ ,  $g_{yy}$  and  $g_{zx}$  data. Migration density with a cut-off less than  $-0.2 \text{ g cm}^{-3}$  density contrast is shown.

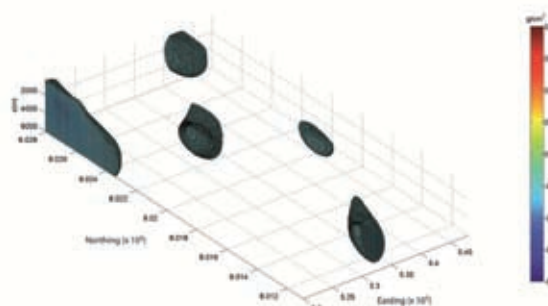


**Figure 11** Volume image of density obtained from 3D smooth inversion with a cut-off less than  $-0.08 \text{ g cm}^{-3}$  density contrast.

was terminated inside salt. Recent discoveries in nearby basins suggest potential for further hydrocarbon discoveries within the Nordkapp Basin (Hokstad, K., Myrland, E.A. and Fotland, B., 2009, Salt imaging in the Nordkapp Basin with electromagnetic data. Presented at AAPG 3-P Arctic Conference and Exhibition, Moscow). Improved seismic imaging changed the structural interpretations of the salt diapirs from what were initially thought of as wide salt stocks with vertical flanks to more complex geometries with broad diapirs overhanging narrow stems. Much of the exploration risk associated with these

structures results from distortions in the seismic imaging, and subsequent ambiguity of the salt isopach.

A full tensor gradient survey was acquired over the Nordkapp Basin with the intent of delineating salt geometry. The Tertiary rocks in the area have a density between  $2.30$  and  $2.38 \text{ g cm}^{-3}$ . The salt diapirs are characterized by negative density contrasts relative to the surrounding sediments and can be identified from the gravity gradiometry data. In this paper, we have focused on data for the Obelix prospect in the southwest of the basin; particularly the G2, F1 and F2 salt diapirs (Figure 6).

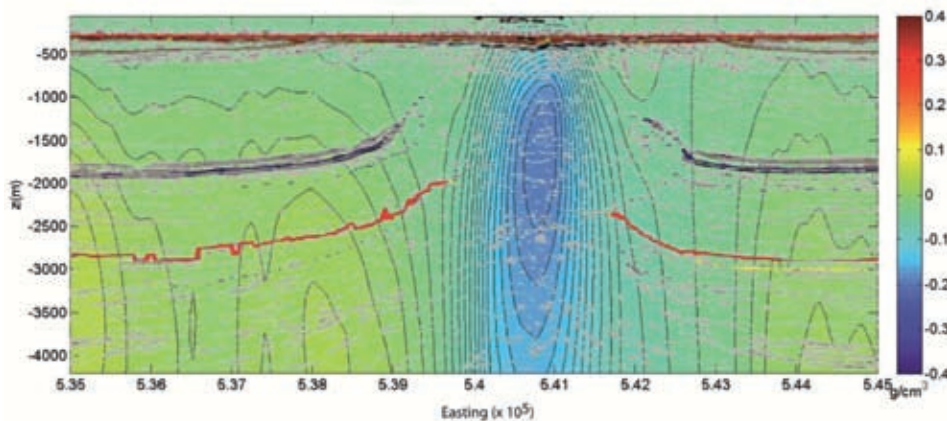


Figure 12 3D gravity gradiometry migration image along profile A-A' co-rendered with the corresponding seismic depth migration image.

In order to obtain a 3D image of the subsurface density distribution, we performed 3D potential field migration of all 48,051 stations of  $g_{xx}$ ,  $g_{yy}$  and  $g_{zz}$  data (Figure 7). We also show the same cross-sections obtained from 3D regularized inversion with smooth and focusing stabilizers in Figures 8 and 9, respectively (Wan and Zhdanov, 2008). The  $28 \text{ km} \times 17 \text{ km} \times 6 \text{ km}$  inversion domain was discretized into 2,856,000 elements of  $100 \text{ m} \times 100 \text{ m} \times 100 \text{ m}$  size. We can see the same typical negative density contrasts in all figures and note how the 3D migration result is nearly identical to the smooth inversion result. In Figure 10, a volume image of the 3D potential field migration result is shown with a cut-off of  $-0.2 \text{ g cm}^{-3}$ , whereas Figure 11 shows a similar volume image of the 3D smooth inversion result with a cut-off of  $-0.08 \text{ g cm}^{-3}$ . When comparing Figures 10 and 11, it is apparent that the smooth inversion result underestimates the density distribution relative to migration. Figure 12 is the 3D gravity migration along profile A-A'. This is co-rendered with the corresponding seismic depth migration image. Salt diapir F2 is clearly identified in both the gravity gradient and seismic migration images.

In terms of computation time, 3D migration required less than one minute on a PC running 32 bit Windows XP with 4 GB of memory. On the same PC, 3D smooth inversion required 3.4 hours and 3D focusing inversion required 25.2 hours. Both 3D inversions ran to a common misfit of 1.9%.

## Conclusions

We have introduced potential field migration as a new method for rapidly interpreting entire surveys of gravity and gravity gradiometry data. This method can naturally be extended to magnetic fields and/or their gradients. For gravity fields and their gradients, we have shown that potential field migration is an integral transformation of the gravity field and/or gradients into subsurface density distributions. Potential field migration is very fast and stable and can be used for rapid imaging with 3D density distributions. We have demonstrated the use of migration for interpreting an entire survey acquired for salt mapping in the Nordkapp Basin of the Barents Sea, and shown how the 3D migration density is effectively equivalent to the 3D density distribution obtained from regularized inversion

with a smooth stabilizer. This novel method of 3D potential field migration also opens the possibility of real-time imaging of potential field data for a wide variety of applications.

## Acknowledgements

Support for this research has been provided by TechnoImaging and The University of Utah's Consortium for Electromagnetic Modeling and Inversion (CEMI). We thank Brian Farrelly and Statoil for providing the Nordkapp Basin gravity gradiometry data and for permission to publish the results of interpretation of this data.

## References

- Berkhout, A.J. [1980] *Seismic Migration*. Elsevier, Amsterdam.
- Claerbout, J.F. [1985] *Imaging the Earth's Interior*. Blackwell, Oxford.
- Fedi, M. [2007] DEXP: A fast method to determine the depth to the sources of potential fields. *Geophysics*, 72, L1-L11.
- Li, Y. [2001] 3D inversion of gravity gradiometer data. *71<sup>st</sup> SEG Annual Meeting*, Expanded Abstracts, 20, 1470-1473.
- Nilsen, K.T., Vendeville, B.C. and Johansen, J.T. [1995] Influence of regional tectonics on halokinesis in the Nordkapp Basin, Barents Sea. In: Jackson, M.P.A., Roberts, D.G. and Snelson, S. (Eds.) *Salt Tectonics: a Global Perspective*. AAPG, Tulsa, 413-436.
- Schneider, W.A. [1978] Integral formulation for migration in two and three dimensions. *Geophysics*, 43, 49-76.
- Strakhov, V.N. [1970] Some aspects of the plane gravitational problem. *Izvestiya Akademii Nauk SSSR Fizika Zemli*, 12, 32-44. (In Russian).
- Wan, L. and Zhdanov, M.S. [2008] Focusing inversion of marine full-tensor gradiometry data in offshore geophysical exploration. *78<sup>th</sup> SEG Annual Meeting*, Expanded Abstracts, 27, 751-755.
- Zhdanov, M.S. [1988] *Integral Transforms in Geophysics*. Springer-Verlag, Berlin.
- Zhdanov, M.S. [2002] *Geophysical Inverse Theory and Regularization Problems*. Elsevier, Amsterdam.
- Zhdanov, M.S. [2009] *Geophysical Electromagnetic Theory and Methods*. Elsevier, Amsterdam.
- Zhdanov, M.S., Ellis, R.G. and Mukherjee, S. [2004] Three-dimensional regularized focusing inversion of gravity gradient tensor component data. *Geophysics*, 69, 925-937.

Received 2 August 2010; accepted 31 August 2010.